# Imperfections of slender glulam beams

Prof. Dr.-Ing. Ulrike Kuhlmann, Head of Institute

Janusch Töpler, M.Sc., Scientific Researcher

Institute of Structural Design, University of Stuttgart

# 1    Introduction

Imperfection assumptions are essential for the design verification of imperfection-sensitive (slender) timber members and adjacent structural elements, including roof bracings and fork bearings (LARSEN (1977)), (KUHLMANN & HOFMANN (2016)). However only few imperfection measurements concerning timber buildings exist (BRÜNINGHOFF (1973)), (DIETSCH & HENKE (2010)), (EHLBECK & BLAß (1987)), (KESSEL & KÜHL & HALL (2015)), yet there is a lack of sufficient data regarding slender roof girders. Furthermore, the equivalent imperfections in EN 1995-1-1 (2004), on which the verifications of in-plane buckling and lateral torsional buckling are based, are inconsistent (e.g. initial bow imperfections for glulam included in the effective length method in-plane buckling ($k_c$-method): $e_y \approx L/1100$ and lateral torsional buckling ($k_{crit}$-method): $e_y \approx L/288$ to $L/577$)

(EHLBECK & BLAß (1987)), (HEIMES-HOFF (1986)). Consequently, due to the possibility of conservative assumptions of imperfections, load-bearing capacity reserves may be expected in the verification of timber members at risk of lateral torsional buckling, when using the effective length method or design verification according to second order theory. Also, in achieving a more economical design of fork bearings, there is a lack of know-



*Figure 1.1. On-site imperfection measurement with a laser scanner Leica ScanStation P20 (building 2020-KW34).*

ledge referring to the assembly tolerances of long-spanning roof structures (KUHLMANN & HOFMANN (2013)).

Within a DIBt research project (KUHLMANN & TÖPLER (2021 b)), measurements of the assembly tolerances of timber building structures were carried out by the Institute of Structural Design from 2020 to 2021 (Figure 1.1), in order to create a database of geometric imperfections of slender glulam beams and to develop consistent proposals for equivalent imperfections. These should contribute to the current revision of EN 1995-1-1 (2004) and the preparation of the new European standard "Execution of Timber Structures".

This paper presents the results of imperfection measurements on 139 slender glulam beams in 13 timber buildings using a laser scanner (Figure 1.1) conducted in 2020. Using numerical methods, equivalent imperfections and torsional moments at the fork bearings are determined. The results are compared with current design rules.

# 2    Imperfection measurements

## 2.1    General

As part of the DIBt research project DIBt - ZP 52-5-13.194, assembly tolerances of approximately 25 timber buildings shortly after assembly have been determined with a laser scanner from 2020 to 2021. Buildings with glulam beams made of softwood and beam-columns made of beech LVL were surveyed. The measurements were carried out in cooperation with the Institute for Photogrammetry at the University of Stuttgart. This paper reports on the measurement results of the glulam beams.

Detailed explanations can be found in the interim report of the research project (KUHLMANN & TÖPLER (2021 b)).
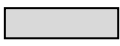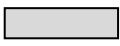
## 2.2    Measurement programme, setup and execution

### 2.2.1    Measurement programme

Table 2.1 lists the 13 buildings with 139 slender glulam beams reported. To ensure the representativeness of the sample of timber buildings, typical beam geometries (span L, cross-sectional dimensions H and W and beam shape) and material grades commonly used in construction practice in the DACH (Germany, Austria, Switzerland) region were covered. The timber buildings' elements were fabricated und erected by different manufacturers and assembly companies.

All buildings were single-storey industrial halls with roof constructions made of slender glulam beams (see e.g. Figure 1.1). The beam span of the evaluated members ranged between 6.9 m and 42.4 m, cross-sectional height between 0.69 m and 2.68 m and cross-sectional width between 0.14 m and 0.26 m. Material grades of the beams were GL 24h and GL 28c and roof bracings were realised by means of steel/timber diagonals, glulam roof panels or fixed columns.

*Table 2.1. Measured buildings with slender glulam beams.*

| Building | Beam shape | Span [m] | Cross-sectional height/width | Material | Bracing system | Location (in Germany) |
|---|---|---|---|---|---|---|
| 2020-KW23 | | 14.5 | 5.1 | GL 28c | Steel diagonals | 73278 Schlierbach |
| 2020-KW27 | | 29.6 | 12.2 | GL 24h | Timber diagonals | 84359 Simbach a. Inn |
| 2020-KW32 | | 23.6 | 9.0 | GL 28c | Timber diagonals | 74595 Langenburg |
| 2020-KW33 | | 17.9 | 8.8 | GL 28c | Steel diagonals | 84577 Tüßling |
| 2020-KW34 | | 13.1 - 17.5 | 6.5 - 12.6 | GL 24h | Timber diagonals + fixed columns | 89616 Rottenacker |
| 2020-KW38_1.1 | | 17.4 | 5.0 | GL 28c | Glulam roof panel | 68199 Mannheim |
| 2020-KW38_1.2 | | 9.9 | 3.6 | GL 24h | Glulam roof panel | 68199 Mannheim |
| 2020-KW38_1.3 | | 10.0 | 3.8 | GL 24h | Glulam roof panel | 68199 Mannheim |
| 2020-KW38_1.4 | | 6.9 | 2.9 + 4.8 | GL 24h | Glulam roof panel | 68199 Mannheim |
| 2020-KW38_2 | | 42.4 | 10.6 | GL 28c | Timber diagonals | 86199 Augsburg |
| 2020-KW45_1.1 | | 23.5 | 9.2 | GL 28c | Steel diagonals | 67112 Mutterstadt |
| 2020-KW45_1.2 | | 26.5 | 9.3 | GL 28c | Steel diagonals | 67112 Mutterstadt |
| 2020-KW47 | | 20.8 | 6.8 | GL 24h | Timber diagonals | 91320 Ebermannstadt |

The measurements were taken directly after assembly and alignment of the timber structures. In some cases, the structures were loaded by roofing and wall cladding in addition to their self-weight. The influence of wind actions during the measurement can be neglected, as the estimated Beaufort number describing the wind speed was always ≤ 5 (fresh breeze).

The measured geometry of the structures thus particularly includes influences from assembly, transport and production. Influences from the loading, the long-term behaviour and slip within the connections, which might occur at the first significant loading of the roof structures, are not included in the measurement results (or only included to a negligible extent).

## 2.2.2   Measurement setup and execution

The measurements were carried out with a Leica ScanStation P20 laser scanner (Figure 1.1), which records measurement points in a grid of 3.1 mm x 3.1 mm when assuming a distance of 10 m (Leica Geosystems AG (2013)). Using several measurement locations per building, a 3D point cloud of the entire structure was generated from the

ground surface (Figure 2.1). The total measurement time per building was between 1.5 and 5 hours.

In addition, the air temperature and humidity and, if possible, the wood moisture content were determined in at least three structural elements per building with a Trotec T2000 multifunctional measuring device. Furthermore, information was collected concerning the building structure, material, manufacture, transport, assembly process, weathering, surface quality and any damage to the timber members.

## 2.3    Measurement results

### 2.3.1    Evaluation

The measurement error of a measurement point at a distance of the laser scanner to the object of approx. 15 m is specified in the laser scanner manual as approx. 1 mm in the x, y and z directions (position accuracy and range noise) (LEICA GEOSYSTEMS AG (2013)). This coincides with observed deviations when evaluating the measurement results of individual point coordinates. Therefore, in the evaluation, average values of the point coordinates of 200 to 1000 measuring points were always calculated, whereby the accuracy of the averaged point coordinates could be increased to less than 0.1 mm (at a confidence level of 90 % according to (FISCHER (2003)) in the x, y and z directions. Since this is a random error, with expected horizontal bow imperfections $e_y$ of the beams of approx. L/1000 = 6.9 mm (Table 2.1, min L = 6.9 m), the measuring accuracy of the laser scanner is sufficient.

The point clouds (Figure 2.1) were automatically evaluated using Matlab software. The coordinate system used is shown in Figure 2.2. The results of the evaluation are the y and z coordinates of the beam axis over the beam length (bow imperfections $e_y$) and the torsion of the cross-section around the x-axis (twist imperfections $e_\vartheta$). Figure 2.3 shows examples of measured horizontal bow imperfections $e_y$ and Figure 2.5 displays the twist imperfections $e_\vartheta$ over the beam length (x direction). $e_\vartheta$ describes the twist of a cross-section around the x-axis without units (gradient of a straight line to the vertical).
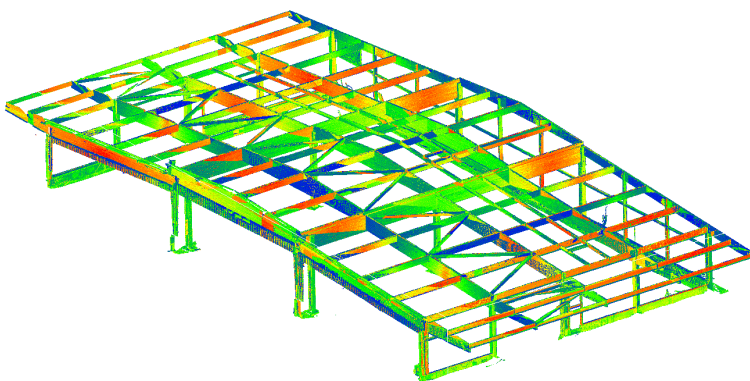


Figure 2.1. Point cloud from laser scan measurements (building 2020-KW34), the colour represents the intensity of the laser signal and has no further meaning.
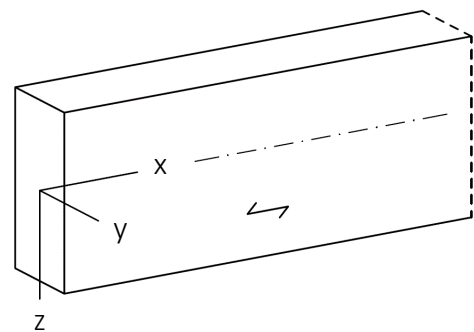


Figure 2.2. Generally used coordinate system.

### 2.3.2 Results

Figure 2.3 shows typical curves of the measured **horizontal bow imperfections $e_y$** of the beam axis over the beam length (x direction). The ideal planned beam position with the two supports " x " is shown as a dash line " - - ". Essential observations when assessing the bow imperfection curves are:

- The shape of the bow imperfection over the beam length usually (122 of 139 beams) corresponded approximately to a sinusoidal or parabolic curve (Figure 2.3 (b) and (d)). In some cases (11 of 139 beams) a bump shape occurred (Figure 2.3 (a)). However, in a few cases (6 of 139 beams) a change in the sign of the bow imperfections $e_y$ was observed at a point of application of a compression purlin (Figure 2.3 (c)). In general, the bow imperfection curves could be represented by a sinusoidal half-wave (Kuhlmann & Töpler (2021 b)).

- Over the beam length, discontinuity points / outliers of individual y coordinates were sometimes observed, which were attributed to local defects (e.g. knotholes) or connected members such as purlins. These were neglected in the evaluation.

Figure 2.4 shows the maximum values of the measured horizontal bow imperfections $e_y$ of 139 glulam beams, separated by buildings (see also Table 2.1). Additionally the results of measurements on 7 beams of (DIETSCH & HENKE (2010)) are added in the diagram. The x-axis displays the beam span (distance between the supports of the structural system) and the y-axis exhibits the bow imperfections $e_y$. Each data point represents the maximum measured horizontal bow imperfection (not necessarily at midspan, Figure 2.3) of a beam. In addition, the equivalent bow imperfection for calculations according to second order theory (EN 1995-1-1 (2004)) with L/400, and the value



*(a) Building 2020-KW32 - Beam axis 7*

*(b) Building 2020-KW33 - Beam axis 4*

*(c) Building 2020-KW38_2 - Beam axis 25*
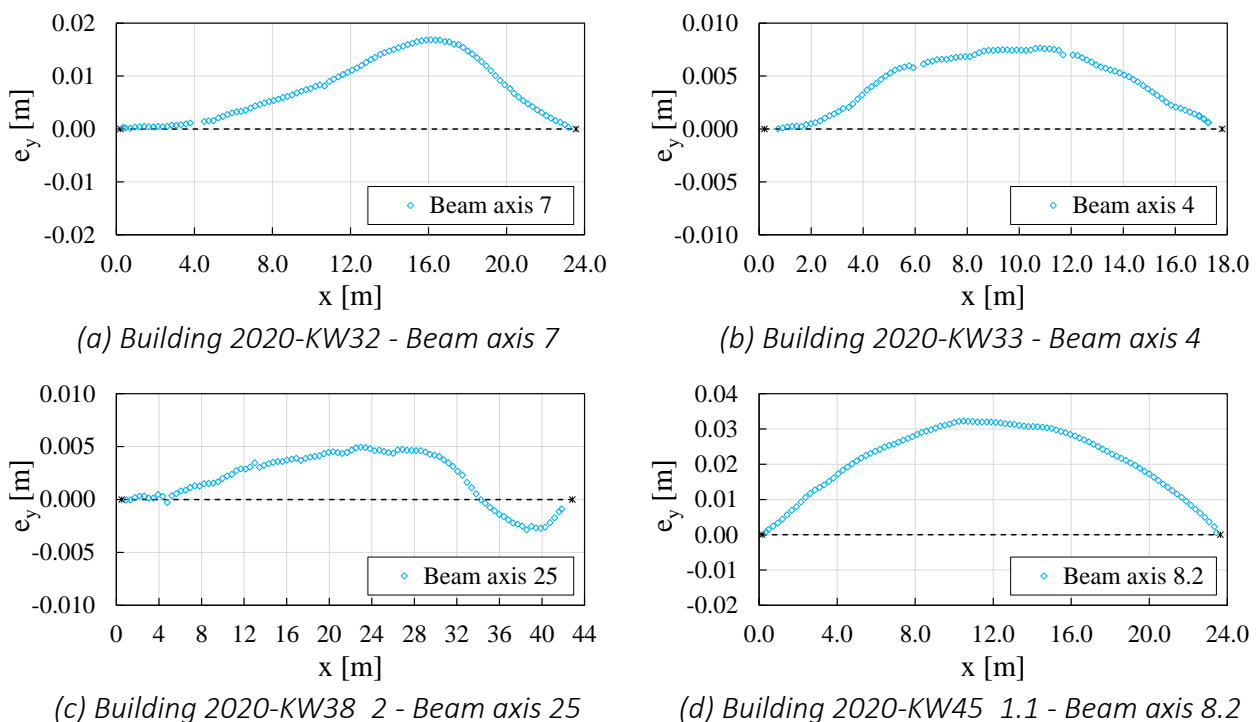
*(d) Building 2020-KW45_1.1 - Beam axis 8.2*

Figure 2.3. Typical curves of the measured horizontal bow imperfections $e_y$, or elevated top view of the beams, with x-axis as longitudinal axis.

L/1000 are displayed. All measured bow imperfections $e_y$ were below L/400. A maximum bow imperfection $e_y$ of L/1000 was exceeded by 18 of the 139 glulam beams (13 %). For buildings with beams with measured $e_y$ > L/1000, assembly difficulties were reported due to small tolerances of connectors (2020-KW27), one of two roof bracings was not aligned according to generally accepted standards (2020-KW45_1.1), or the beams were braced by glulam roof panels and therefore could not be aligned horizontally during assembly (2020-KW38_1.1). When looking at the scatter band, the linear relationship between bow imperfection $e_y$ and beam span assumed in EN 1995-1-1 (2004) is generally confirmed. A significant influence of the horizontal beam stiffness on the measured bow imperfections $e_y$ could not be found.

The measurement results (DIETSCH & HENKE (2010)) are somewhat less favourable (Figure 2.4), which could be due to the fact that the 7 measured beams were not only loaded by their self-weight and were partly already subjected to long-term influences.

Figure 2.5 shows typical curves of the measured **twist imperfections $e_\vartheta$** around the x-axis over the beam length (x direction). A positive twist $e_\vartheta$ means that the measured y coordinate of the upper edge of the beam is greater than that of the lower edge of the beam (see Figure 2.6). The ideal planned beam position with the two supports " x " is shown as a dash line " - - ". Essential observations when assessing the twist imperfection curves are:

- Unlike the bow imperfection curves, the shape of the twist imperfections over the beam length cannot be assigned to a generally valid curve shape.

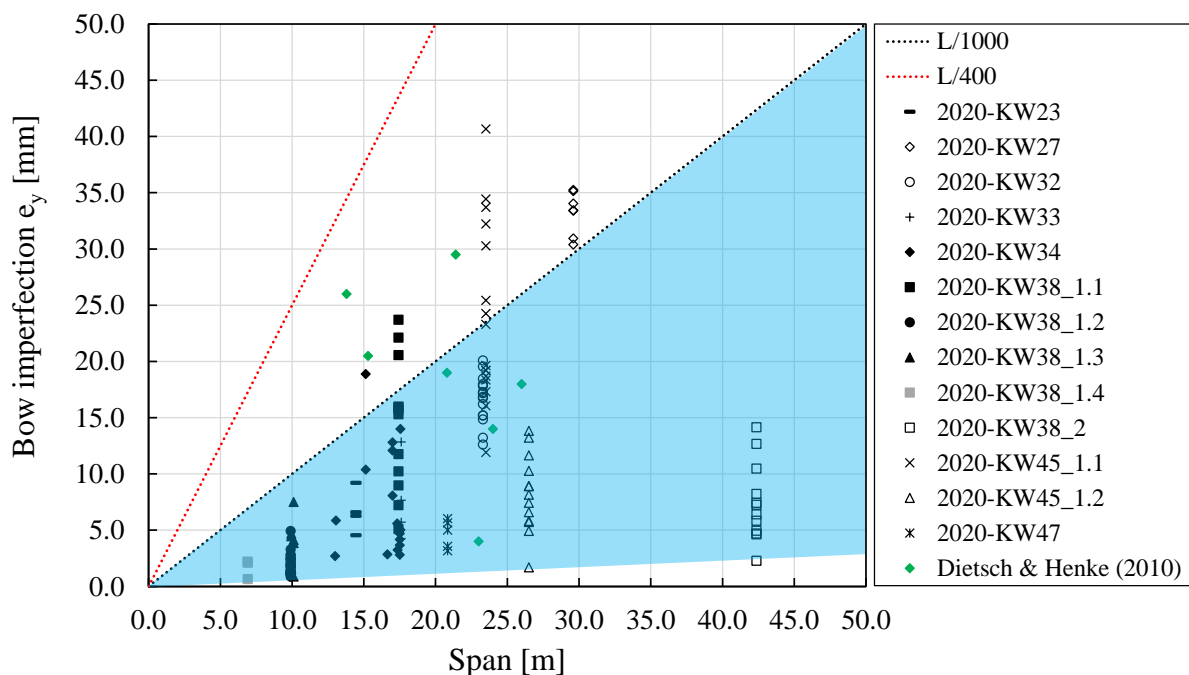- The maximum twist imperfection often occurred at supports (104 of 139 beams),



Figure 2.4. Maximum measured horizontal bow imperfections of 139 glulam beams with scatter band (blue) plotted for 87 % of the measured values, measurement results of 7 beams of (DIETSCH & HENKE (2010)) added, span shown on the x-axis and bow imperfections on the y-axis, each data point representing one beam.

especially if the fork bearings were designed as a reinforced concrete pockets.

- The shape of the twist imperfections along the beam length was in some cases (23 of 139 beams) approximately sinusoidal or parabolic (Figure 2.5 (a)). But in general, the maximum $e_\vartheta$ was either at one support (43 beams, Figure 2.5 (b)), at both supports with the same sign (44 beams, Figure 2.5 (c)), or at both supports with opposite signs (17 beams, Figure 2.5 (d)). Not all of the beams could clearly be assigned to one of these cases.

Figure 2.6 shows the maximum values of $e_\vartheta$ x H (differences of the measured horizontal displacements of the top edge to the bottom edge of the beam) of the 139 glulam beams, separated by buildings (see also Table 2.1). Additionally the results of measurements on 6 beams of (DIETSCH & HENKE (2010)) are added in the diagram. The x-axis displays the beam span (distance between the supports of the structural system) and the y-axis exhibits $e_\vartheta$ x H (twist imperfection x beam height). Each data point represents the absolute maximum value (not necessarily at midspan, Figure 2.5) of a beam. The measured values show increasing horizontal differential deformations $e_\vartheta$ x H between the top and bottom edge of the beam as the span increases. This relationship is also shown by the regression line $e_\vartheta$ x H = 0.0005 x L, which results from the evaluation of the data. The measurement results (DIETSCH & HENKE (2010)) fit well into the overall picture of the own measurement results.

The correlation $e_\vartheta$ = 0.05 x Width / Height found by (LARSEN (1977)) on solid wood test specimens cannot be confirmed by the measurement results.

In Figure 2.6 measured values of beams with fork bearings not made of reinforced concrete pockets (e.g. fork bearing by means of lateral timber plates), are marked in blue.

(a) Building 2020-KW23 - Beam axis 2

(b) Building 2020-KW32 - Beam axis 5

(c) Building 2020-KW33 - Beam axis 3

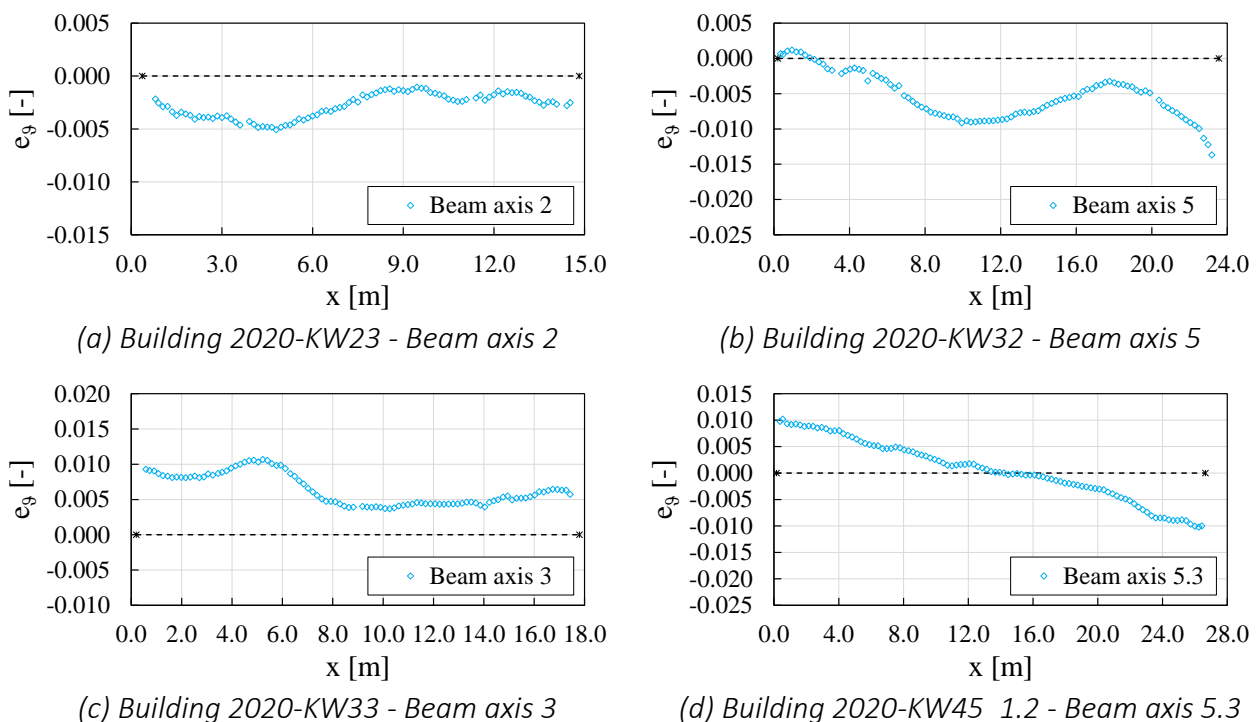(d) Building 2020-KW45_1.2 - Beam axis 5.3

Figure 2.5. Typical curves of the measured twist imperfections $e_\vartheta$ around the x-axis, with x-axis as longitudinal axis.

Such a design seems to favour smaller assembly tolerances with regard to the twist imperfections.

# 3 Numerical simulations

## 3.1 General

The numerical calculations were executed with a FE-model in Abaqus/CAE 2018. The aim being to investigate the stability behaviour of the measured beams and to determine equivalent imperfections, as well as to examine the torsional moments at the supports. For each measured beam, calculations of eigenvalues (model 1), computations with measured imperfections (model 2) and with equivalent imperfections (model 3) have been carried out.

## 3.2 Numerical modelling and calculation procedure

In Figure 3.1 the numerical model of the building 2020-KW23 is displayed. The beam was modelled according to the ideal planned geometry. The horizontal stabilising influence of the roof bracing was taken into account by an equivalent beam, where the stiffness was determined based on (KESSEL & SIEDER & KREUZINGER (2020)). The stiffness of the purlins was mapped by equivalent springs acting only in y direction. For the glulam beam, 20-node quadratic brick elements with a mesh fineness of 100 elements in length, 10 elements in height and 8 elements in width were chosen. An orthotropic material model with mean material properties according to EN 14080 (2013), Poisson's ratios according to (NEUHAUS (1981)), bilinear elasto-plastic material behaviour under compression along the grain and linear elastic material behaviour under tension along
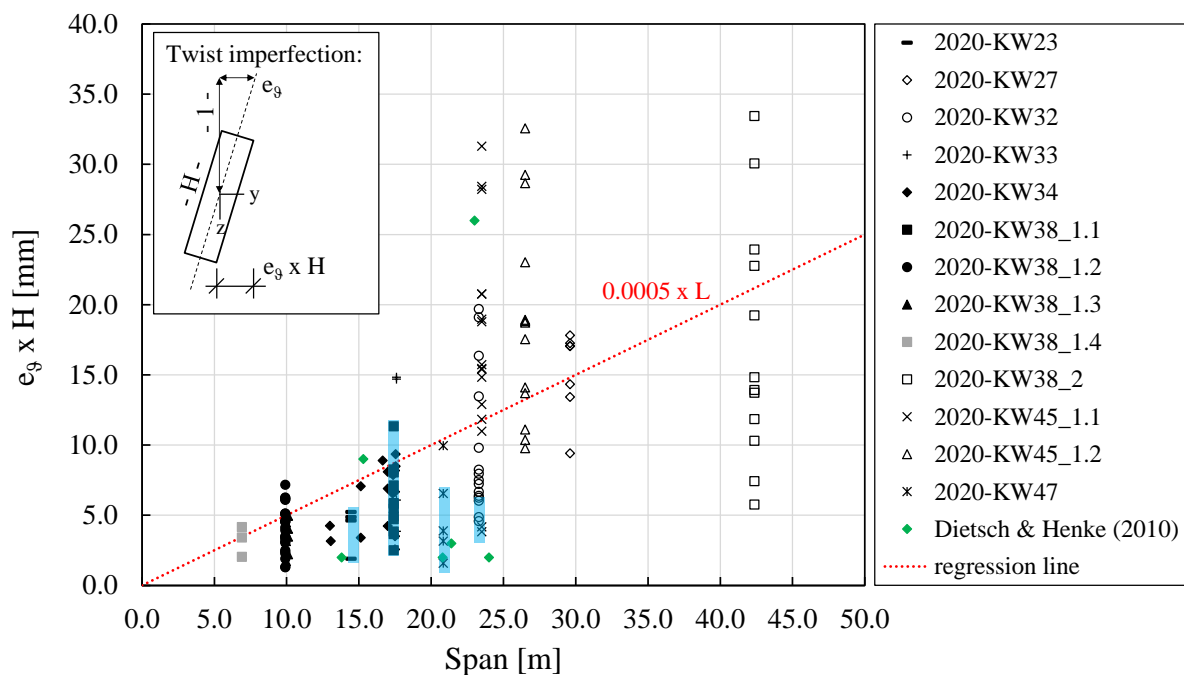
Figure 2.6. Maximum measured twist imperfections around the x-axis of 139 glulam beams, measurement results of 6 beams of (DIETSCH & HENKE (2010)) added, span shown on the x-axis and $e_\vartheta$ x H on the y-axis, each data point representing one beam, blue marked are measured values of beams with fork bearings not made of reinforced concrete pockets.
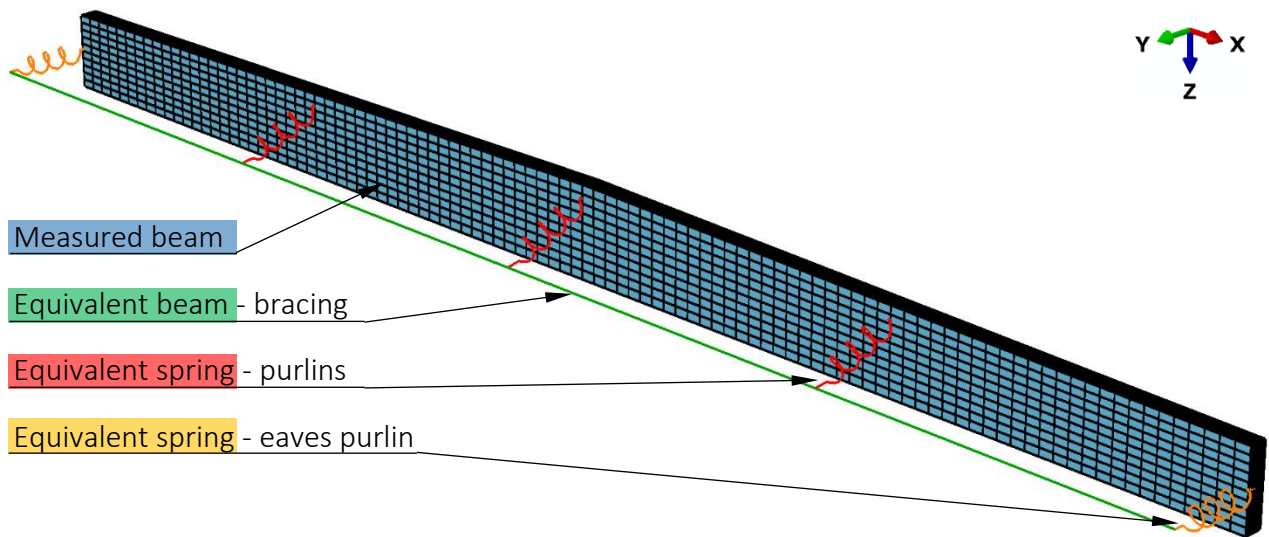
*Figure 3.1. Numerical model of the double-tapered beams in building 2020-KW23.*

the grain was used. The grain direction was chosen parallel to the bottom edge of the beam, also for curved beams. The load was applied by means of a line load at the upper edge of the beam. The calculations on model 2 and 3 were performed as geometrically and materially non-linear analysis with imperfections (GMNIA, prEN 1993-1-14 (2021)). The verification of the numerical models was achieved according to prEN 1993-1-14 (2021) (see also (KUHLMANN & TÖPLER (2021 a)).

In model 1 no imperfections and purely elastic behaviour were considered. Using model 1, the eigenvalues and eigenmodes of a beam were determined and the relative slenderness ratio $\lambda_{rel,m}$ and resulting $l_{ef,m}$ were evaluated (EN 1995-1-1 (2004)).

In model 2 the measured imperfections were assumed. By means of model 2, the maximum load-bearing capacity and associated line load $q_{max}$ of a beam, at which the tensile stress $\sigma_x$ reaches the characteristic bending strength $f_{m,k}$ (EN 14080 (2013)), was computed.

In model 3 the equivalent imperfections were applied. Due to the possible eigenmodes, both global equivalent imperfections (wavelength / 2 = beam span), local equivalent imperfections (wavelength / 2 = distance between purlins) and a superposition of both imperfections were included in preliminary investigations (Figure 3.2). While model 2 obtained the line load $q_{max}$ which was then applied in model 3. The corresponding bending stresses and the ratio $\sigma_x / f_{m,k}$ (= utilization $\mu_x$), which indicates
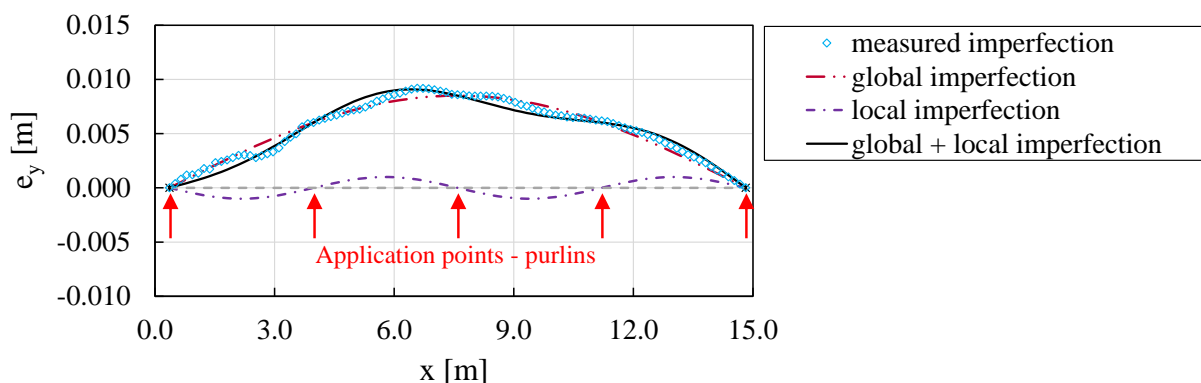


*Figure 3.2. Bow imperfections for the numerical modelling, beam axis 2 in building 2020-KW23.*

to what extend the approach of the equivalent imperfections is suitable to represent the real beam behaviour (with measured imperfections), were determined.

This procedure was carried out for all 139 beams. Additionally the torsional moments at the supports $M_x$ were derived for all of the beams based on model 2 and 3.

## 3.3 Results and evaluation

### 3.3.1 General

The horizontal stiffness of the roof bracing on the measured buildings proved to be substantial, so that for the bending stress verification the governing eigenmode corresponded to a superposition of global and local imperfections (multiwave over the beam length; $0.69 \leq l_{ef,m} / a_{purlins}$ = effective length / distance between purlins $\leq 1.61$).

In consultation with structural engineers, the assumption of combined global and local equivalent imperfections similar to Figure 3.2 seems to be too complex for design calculations. Therefore, for the calculations with equivalent imperfections (model 3), only global equivalent bow and twist imperfections (no local ones) were assumed (Figure 3.2). The differences in the load-bearing behaviour between model 2 and model 3 thus also include the influence of local imperfections between the application points of the purlins. The amplitudes of the global equivalent imperfections were chosen so that the area integral of the equivalent imperfections over the beam length corresponded to the area integral of the measured imperfections.

### 3.3.2 Equivalent imperfections

Table 3.1 illustrates the summarised results of the numerical calculations of the 139 beams. It can be demonstrated that with the chosen approach for the equivalent imperfections (model 3), almost identical utilisations $\mu_x = \sigma_x / f_{m,k}$ have been determined with computations considering measured imperfections (model 2). The mean utilisation $\mu_{x,Mz}$ (caused by bending moments around the weak axis $M_z$) is approximately 15 % smaller in model 3 than in model 2, which is due to the neglect of local imperfections. However, since the share of utilisation $\mu_{x,Mz}$ in the total utilisation $\mu_x$ is a maximum of 26 %, this is not significant. In general, the assumed equivalent imperfections are well suited to represent the load-bearing behaviour of the measured beams for bending.

Table 3.1. Numerically for 139 beams determined mean, min, max and COV values of the relative slenderness ratio $\lambda_{rel,m}$ and the maximum utilisation of the bending stress in x-direction $\mu_x$, utilisation separated for the contributions of $M_y$ and $M_z$.

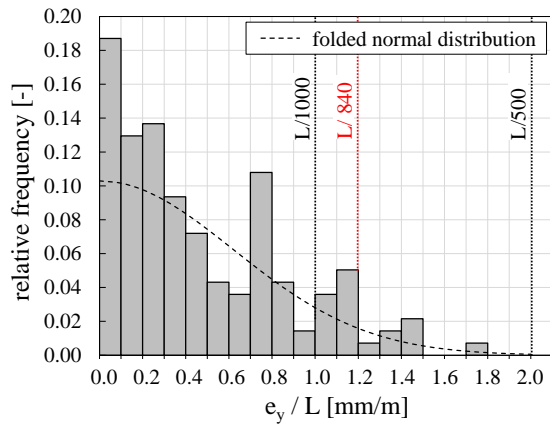| | $\lambda_{rel,m}$ | Model 2 | | | Model 3 | | |
| --- | --- | --- | --- | --- | --- | --- | --- |
| | | $\mu_x = \sigma_x / f_m$ | $\mu_{x,My}$ | $\mu_{x,Mz}$ | $\mu_x = \sigma_x / f_m$ | $\mu_{x,My}$ | $\mu_{x,Mz}$ |
| Mean | 0.79 | 1.00 | 0.94 | 0.06 | 0.99 | 0.94 | 0.05 |
| Minimum | 0.52 | 1.00 | 0.77 | 0.01 | 0.90 | 0.77 | 0.01 |
| Maximum | 1.01 | 1.00 | 0.99 | 0.23 | 1.05 | 0.99 | 0.26 |
| COV | 0.16 | 0.00 | 0.05 | 0.84 | 0.02 | 0.05 | 0.94 |

Figure 3.3. Frequency distribution of the computed equivalent bow imperfections $e_y$ in relation to the beam span L of 139 glulam beams.
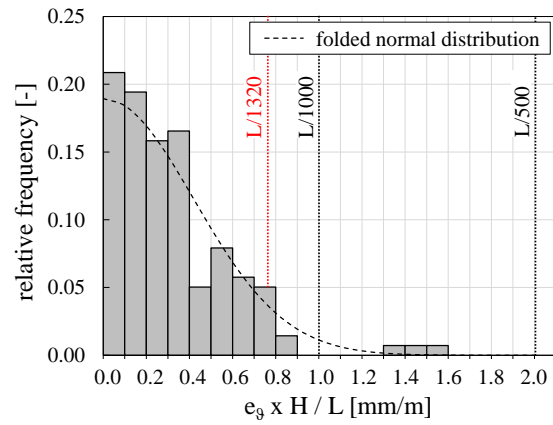
Figure 3.4. Frequency distribution of the computed equivalent twist imperfections $e_\vartheta \times H$ (beam height) in relation to the beam span L of 139 glulam beams.

Figure 3.3 and Figure 3.4 display the frequency distributions of the absolute values of the equivalent bow and twist imperfections $e_y / L$ and $e_\vartheta \times H / L$. A folded normal distribution represents a good approximation of the density functions. The 95 % quantile values of the equivalent imperfections are:

95 % quantile:   $e_y / L$     = 1.19 mm/m $\triangleq$ L / 840     (bow imperfections)

$e_\vartheta \times H / L$ = 0.76 mm/m $\triangleq$ L / 1320   (twist imperfections)

### 3.3.3   Torsional moment at the supports

Figure 3.5 presents the maximum torsional moments $M_x$ at the supports per building determined using model 2 ($M_{x,measured}$) and model 3 ($M_{x,equivalent}$) with measured or equivalent imperfections. In addition, the diagram contains calculation results accord-
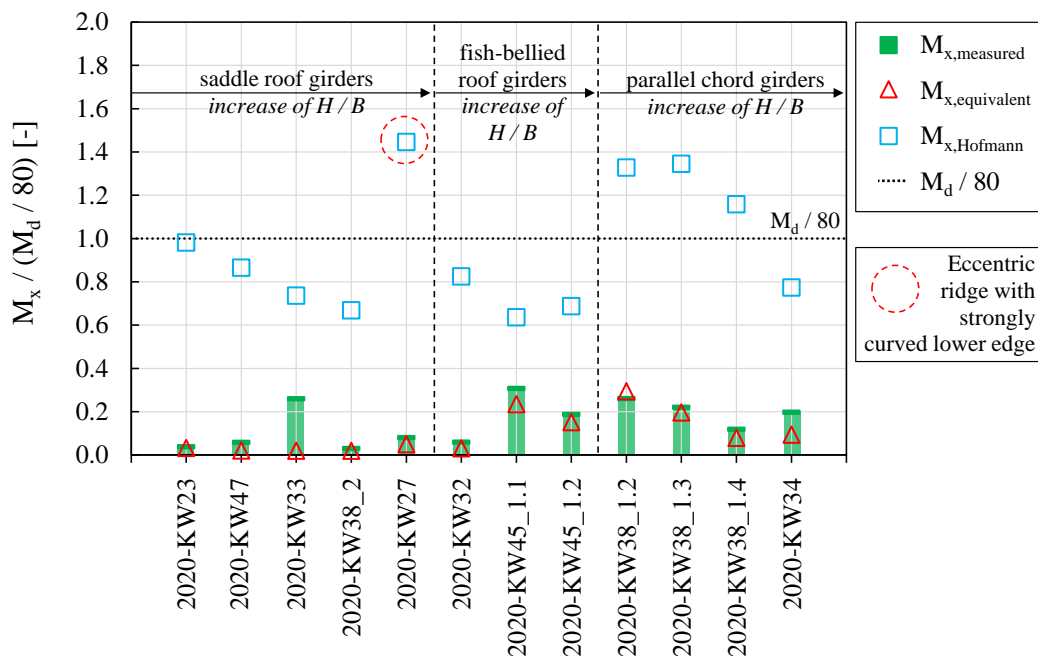


Figure 3.5. Numerically, according to DIN EN 1995-1-1/NA (2013) and (KUHLMANN & HOFMANN (2016)) determined maximum torsional moments $M_x$ at the supports, per building, normalised to $M_d / 80$.

ing to the design approach in DIN EN 1995-1-1/NA (2013) with $M_x = M_d / 80$ and the results of the approaches ($M_{x,Hofmann}$) proposed by (KUHLMANN & HOFMANN (2016)). The data in Figure 3.5 are sorted by the beam shape and the ratio of beam height to width H / B and for comparability normalised to $M_d / 80$.

The major differences between $M_{x,measured/equivalent}$ and $M_{x,Hofmann}$ result from the different imperfection assumptions. According to EN 1995-1-1 (2004), bow imperfections of $e_y = L/400 + L/500$ were assumed in (KUHLMANN & HOFMANN (2016)), whereas the maximum measured bow imperfection was $e_y = L/578$ (2020-KW45_1.1). This is also reflected in the difference at building 2020-KW45_1.1 between $M_{x,measured}$ and $M_{x,Hofmann}$, which is approximately a factor of 2.

Compared to $M_d / 80$, the more accurate approaches of (KUHLMANN & HOFMANN (2016)) and the numerical calculations presented here take into account the influence of the beam shape and the cross-sectional ratio H / B.

It is evident that the imperfection assumptions in the current approaches for $M_x$ are conservative. A revision of the design rules based on the generated database of measured imperfections and the more accurate approaches of (KUHLMANN & HOFMANN (2016)) is recommended.

# 4    Summary and outlook

The assembly tolerances have a decisive influence on the design of roof structures with slender glulam beams, yet there is a lack of sufficient data regarding these structures.

Chapter 2 reports on the results of imperfection measurements on 13 roof structures with 139 glulam beams as part of the research project DIBt - ZP 52-5-13.194 (KUHLMANN & TÖPLER (2021 b)). The measured horizontal bow imperfections $e_y$ of the beams were always smaller than L/400 assumed in EN 1995-1-1 (2004) and in 87 % of the cases smaller than L/1000. Likewise significant twist imperfections $e_\vartheta$ around the longitudinal axis could be determined for most of the beams. The horizontal displacement from the upper edge to the lower edge of a beam was on average $e_\vartheta$ x H = 0.0005 x L. Twist imperfections $e_\vartheta$ of beams with fork bearings designed as reinforced concrete pockets were generally larger than with fork bearings made of timber.

It is demonstrated in Chapter 3 by numerical calculations on the 139 measured glulam beams that, assuming sinusoidal equivalent imperfections where the area integral corresponds to the one of the measured imperfections, very similar load-bearing capacities can be determined numerically, compared to calculations with measured imperfections. This may form the basis of recommended values for the new Eurocode 5. Additionally, it should be emphasised that the stiffness of the horizontal bracing of the girders, as well as the fork bearings, have a decisive influence on the load-bearing behaviour (KUHLMANN & HOFMANN (2016)).

The evaluation of the measurement results will continue. In addition to the completion of the evaluation shown in this paper, other possibly systematic effects such as the

assembly procedure, the bracing system, the beam shape, a group effect of several parallel girders, the long-term behaviour and material scatter will be investigated. Possible recommendations will also concern the reduction of tolerances in execution.

# 5 Acknowledgements

# 6 References

Brüninghoff, H. (1973): Spannungen und Stabilität bei quergestützten Brettschichtholzträgern (in German). Dissertation, University of Karlsruhe.

DIN EN 1995-1-1/NA (2013): Nationaler Anhang – National festgelegte Parameter – Eurocode 5: Bemessung und Konstruktion von Holzbauten – Teil 1-1: Allgemeines – Allgemeine Regeln und Regeln für den Hochbau. German Institute of Standardization (DIN), Berlin.

Dietsch, P. & Henke, K. (2010): Verformungsmessungen an weitgespannten Brettschichtholzträgern zur Ermittlung horizontaler Verformungen (in German). Research report, Technical University of Munich.

Ehlbeck, J. & Blaß, H. J. (1987): Zuverlässigkeit von Holzdruckstäben (in German). Research report, University Fridericiana Karlsruhe.

EN 1995-1-1 (2004): Eurocode 5: Design of timber structures – Part 1-1: General – Common rules and rules for buildings. European Committee for Standardization (CEN), Brussels, with corrections and amendments + AC:2006 and A1:2008.

EN 14080 (2013): Timber structures - Glued laminated timber and glued solid timber - Requirements. European Committee for Standardization (CEN), Brussels.

Fischer, L. (2003): Charakteristische Werte - ihre Bedeutung und Berechnung (in German). Bauingenieur, 78, p. 179–187.

Heimeshoff, B. (1986): Berechnung und Ausführung von Holzbauwerken (in German). Ingenieur-Holzbau 86 - Fachtagung für Bauingenieure, Stuttgart, Germany.

Kessel, M. H. & Kühl, A. & Hall, C. (2015): Überprüfung und Ergänzung der Imperfektionsannahmen und Montageregeln der DIN EN 1995-1-1 für Nagelplattenkonstruktionen zur Steigerung ihrer Sicherheit und Wirtschaftlichkeit (in German). Research report, Fraunhofer IRB Verlag.

Kessel, M. H. & Sieder, M. & Kreuzinger, H. (2020): Personal contribution by Martin H. Kessel, Mike Sieder and H. Kreuzinger (DE): Bracing of the main girder of a pedestrian bridge. CEN/TC 250/SC 5/WG 3 N 153.

Kuhlmann, U. & Hofmann, R. (2013): Vereinfachte Bemessung von Brettschichtholzträgern variabler Höhe für das Torsionsmoment aus Kippstabilisierung (in German). IGF research project No. 17398 N (Aif/iVTH), Institute of Structural Design, University of Stuttgart.

Kuhlmann, U. & Hofmann, R. (2016): Simplified method to determine the torsional moment due to lateral torsional buckling. INTER, 49-10-2, Graz, Institute of Structural Design, University of Stuttgart.

Kuhlmann, U. & Töpler, J. (2021 a): Analytical and numerical investigations on imperfection-sensitive timber members subjected to combined bending and axial compression. WCTE 2021, Institute of Structural Design, University of Stuttgart.

Kuhlmann, U. & Töpler, J. (2021 b): Imperfektionsmessungen an stabilitätsgefährdeten Holzbauteilen - Zwischenbericht (in German). Research report, DIBt P 52-5- 13.194-2048/19, Institute of Structural Design, University of Stuttgart.

Kuhlmann, U. & Töpler, J. & Gauß, J. & Buchholz, L. (2021): Integrated approach of testing and numerical verifications (IATN). Research project RP 7, DFG Cluster of Excellence "Integrative Computational Design and Construction for Architecture" (IntCDC), EXC 2120/1 – 390831618, Institute of Structural Design, University of Stuttgart, ongoing.

Larsen, H. J. (1977): Laterally Loaded Timber Columns, Tests and Theory. CIB-W18, 8-15-1, Brussels, Belgium.

Leica Geosystems AG (2013): Leica ScanStation P20. User Manual.

Neuhaus, F.-H. (1981): Elastizitätszahlen von Fichtenholz in Abhängigkeit der Holzfeuchtigkeit (in German). Dissertation, Ruhr University Bochum.

prEN 1993-1-14 (14 April 2021): Eurocode 3: Design of steel structures – Part 1-14: Design assisted by finite element analysis (draft version). CEN/TC 250/SC 3/WG 22 N 32.